Accepted Manuscript

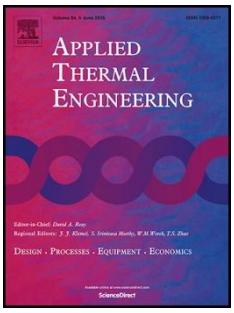

Title: A two-dimensional analytical model for prediction of the radiation heat transfer in open-cell metal foams

Author: Z. Jiang, K. Wang, H. Wu, Y. Wang, J. Du

PII: S1359-4311(15)00963-1
DOI: http://dx.doi.org/doi: 10.1016/j.applthermaleng.2015.09.043
Reference: ATE 7035

To appear in: *Applied Thermal Engineering*

Received date: 15-4-2015
Accepted date: 8-9-2015

Please cite this article as: Z. Jiang, K. Wang, H. Wu, Y. Wang, J. Du, A two-dimensional analytical model for prediction of the radiation heat transfer in open-cell metal foams, *Applied Thermal Engineering* (2015), http://dx.doi.org/doi: 10.1016/j.applthermaleng.2015.09.043.

A Two-dimensional Analytical Model for Prediction of the Radiation Heat Transfer in Open-cell Metal Foams

Z. Jiang[a], K. Wang[a,*], H. Wu[b,**], Y. Wang[a], J. Du[a]

[a,*]Institute of Engineering Thermophysics, Chinese Academy of Sciences
Beijing, 100190, China.

[b,**]Institute of Engineering and Energy Technologies, School of Engineering and Computing,
University of the West of Scotland, Paisley, PA1 2BE, United Kingdom,

Highlights:

- A new 2D explicit analytical model is developed to study the radiation heat transfer.
- A new correction factor is introduced to correct the deviation of specific area.
- The present model has a reasonable precision by comparing with published data.
- The effects of different control factors on the radiation characteristics are evaluated.

Abstract

In this article, a new two-dimensional (2D) explicit analytical model for the evaluation of the radiation heat transfer in highly porous open-cell metal foams is formulated and validated. A correction factor, *C*, is introduced to correct the deviation of the specific area in a simplified manner. Numerical results are compared with the published experimental data and three-dimensional (3D) model proposed in previous works. It reveals that the present two-dimensional model is proved to be relatively accurate in estimating the radiative conductivity for all the investigated structures. In

the current work, the effects of the control parameters, such as the number of order in the iterative procedure, solid emissivity, the temperature difference, shape of solid particle and correction factor on the predictions of radiation characteristics are well discussed.

Keywords: Modelling; Thermal radiation; Porous medium; Open-cell metal foam; Radiation heat transfer.

Nomenclature

a	side length [m]	X, Y	Cartesian coordinates [-]
A_{sf}	specific area [m^{-1}]	***Greek symbols***	
b	bottom face of the unit cell [-]	α_i	dimensional coefficient [-]
C	correction factor [-]	β_i	dimensional coefficient [-]
d	side length of the unit cell [m]	ε	solid emissivity[-]
d_f	diameter of strut [m]	ρ	solid reflectance [-]
d_p	characteristic cell size [m]	σ	Stefan-Boltzmann constant[W/ m^2K^4]
F	configuration factor [-]	ϕ	porosity [-]
H	foam sample thickness [m]	***Subscripts***	
i	sequence of the unit cell [-]	bt	void face b to void face t
J	irradiation from void face[W/m^2]	bj	void face b to solid particle j
k_r	radiative conductivity [W/m K]	c	cold side
l_b	length of bottom void face [m]	h	hot side
l_j	length of solid particle [m]	jk	solid particle j to solid particle k
l_s	length of side void face [m]	jt	solid particle j to void face t
l_t	length of top void face [m]	kt	solid particle k to void face t

N_c	total number of cells [-]	*sj*	void face s to solid particle j
q_r	radiation heat flux [W/m^2]	*st*	void face s to void face t
Q_r	irradiation [m s^{-2}]	***Superscripts***	
s	side face of the unit cell [-]	-	negative direction
t	top face of the unit cell [-]		
T	temperature [K]		

38

39

40 **1. Introduction**

41 Metal foams are extensively used for many industrial applications involving
42 numerous technological fields over more than 50 years due to their attractive physical
43 properties such as, high porosity, large specific surface, flow mixing enhancement,
44 attractive stiffness properties and low cost [1]. Their averaged thermo-physical
45 properties are also important for many applications, e.g., compact heat exchangers [2],
46 solar receivers [3], and catalytic reactors [4]. The main characteristic of the heat
47 transfer in metal foams is dictated by the enhanced effective thermal conductivity
48 (ETC). The ETC used to quantify the magnitude of the heat conduction in metal
49 foams is studied through model prediction [5-13], numerical simulation [14-16] and
50 experimental research [16-18].

51 Previous publications reported on the thermal properties of the metal foams at high
52 temperature where conduction and radiation heat transfer may occur are relatively
53 weak [19]. To overcome the experimental difficulties, Coquard et al. [20] proposed an

innovative method to evaluate the conduction and radiation contribution in metal foams. They developed an identification method using thermograms obtained from laser-FLASH measurements to minimize the discrepancy between experimental and theoretical thermograms. Coquard et al. [19], afterwards, presented a detailed review on the radiation and conduction heat transfer from ambient to high temperature. They also proposed an analytical model for the real foams to predict the conduction and radiation heat transfer at high temperature. Their predicted results agreed well with the experimental results [20].

Several studies have been devoted to the radiation heat transfer in metal foam [21-24]. Coquard et al. [21] modelled the radiation heat transfer in open cell metal foams and closed cell polymer foams utilizing two approaches, i.e., Homogeneous Phase Approach (HPA) and Multi-Phase Approach (MPA). The radiation heat transfer of these two types of foams was investigated using three-dimensional (3D) tomographic images. The calculated results were compared with the results of direct Monte Carlo (MC) simulations and the suitability of the two approaches was then evaluated. Tancrez et al. [22] developed a general method with direct identification of the radiation properties, i.e., absorption, scattering coefficients and phase function of porous medium using Monte Carlo (MC). This method was applied to both sets of Dispersed radius Overlapping Opaque Spheres (DOOS) in a transparent fluid phase and Dispersed radius Overlapping Transparent Spheres (DOTS) in an opaque solid phase. Zhao et al. [23] measured the ETC of metal foams with a range of pore sizes

and porosities between 300 and 800 K. The radiative conductivity was decoupled from the equivalent conductivity due to conduction. As for the equivalent conductivity due to conduction contribution alone, the model proposed in [6] was used. At the same time, Zhao et al. [24] used the Rosseland equation to calculate the equivalent radiative conductivity based on the experimentally obtained spectral transmittance and reflectance. The calculated results were found to be in satisfactory agreement with the experimental data [23].

Although many significant results in the modelling radiation heat transfer of open-cell metal foam have already been obtained, the aforementioned approaches are not quite suitable for engineering applications. Thus, Zhao et al. [25] proposed an explicit analytical model based on the simplified cubic structure. In this model, the fundamental foam parameters and the emission and reflectance in metal foam structure were considered to establish functional relationships between the structure and the radiation characteristics of open-cell metal foams. The calculated equivalent radiative conductivity showed that in general there was a good agreement between the predicted and experimental data. Most recently, as an extension of the simplified analytical approach of [25], Contento et al. [26] made further improvements by recalculating the configuration factors that involved in the dimensionless coefficients and a close agreement between predicted result and measured data was achieved. As the same time, Contento et al. [27] developed a new radiative heat transfer model based on a more realistic Lord Kelvin representation of open cell metal foams instead

of the simplified cubic structure using the same analytical approach. This explicit simple approach that initially proposed by Zhao et al. [25] can be relatively suitable for engineering applications.

Based on the brief literature review, it can be seen that much effort has been made to develop models for the estimation of the radiation heat transfer in open-cell metal foam. From an engineering perspective, however, due to the complex nature of the configuration factors for implementation in three-dimensional modelling, research on modelling radiation heat transfer has been far from complete. More effort needs to be made in this area. In this study, a newly simplified two-dimensional model is proposed and could serve as an efficient alternative to evaluate the radiative characteristics in porous open-cell metal foams for engineering applications. For the assessment of the new model, the comparisons between numerical predictions with experimental data [23] and previously proposed model [25] are carried out.

2. Model description

2.1. Structure simplification

The microstructure of the typical open cell metal foam is shown in Fig. 1. Porous medium such as metal foams has a complex microstructure made up of solid ligaments and pores generally filled with fluid. In order to simplify the analysis of the radiation heat transfer in metal foam, the microstructure can be assumed to consist of randomly oriented cells with characteristic size d_p which are mostly homogeneous in size and shape, whilst the solid of the metal foam can be treated as particles with

117 simple geometry (circle, square and rectangle etc.) distributed in fluid zone regularly
118 or randomly. For the purpose of simplification, the connection of the solid phase of
119 the metal foam can be neglected (Due to the large porosity ($\phi \geqslant 90\%$) of metal foam,
120 thermal radiation in metal foam mainly passes through the void).

121 Based on the above simplification, a new 2D structure with regularly distributed
122 square particles with side length of *a* are selected to develop the analytical model for
123 analysing the radiation heat transfer, as presented in Fig. 2(a). Since the structure is
124 periodic, Fig.2 (b) shows the details of two neighbouring square unit cells. Within
125 each cell, there are four quarters of solid particle at four corners which are labelled
126 with *1-4* respectively. As for the four faces, two side faces are referred as *s*, whereas
127 the top and bottom faces are represented by *t* and *b*. The relationship between *d* and
128 measured d_p based on the same area is shown as:

129 $$d^2 = \frac{\pi}{4} d_p^2 \tag{1}$$

130 $$d = \frac{\sqrt{\pi}}{2} d_p \tag{2}$$

131 Then, *a* is obtained based on the porosity for the two-dimensional structure as:

132 $$\frac{4a^2}{d^2} = 1 - \phi \tag{2}$$

133 $$a = \sqrt{\frac{1-\phi}{4}} d \tag{3}$$

134 here ϕ is the porosity of the metal foam.

135 *2.2. Assumptions*

In order to simplify the heat transfer mechanism in open-cell metal foam, the following major assumptions were made in the derivations of the governing equations:

(i) the diffraction is neglected. The characteristic size of the porous medium is considered to be large compared to the heat radiation wavelengths.

(ii) the solid particles are assumed as grey and opaque since they are metallic, and the void zone is considered as vacuum.

(iii) the surface of the solid particles reflecting diffusely the incident radiation is assumed since the surface roughness at 10 μm scale is being taken into account [26].

(iv) steady-state heat flow is assumed in a specific zone of the metal foam sandwiched between two plates with cold boundary temperature (T_c) for the top plate and hot boundary temperature (T_h) for the bottom plate. Sample is thermally insulated at side walls, which means that there exists a radiation heat flux in the positive Y direction.

(v) it is assumed that the radiation is decoupled from the conduction and the temperature varies linearly with Y direction [25].

(vi) temperature difference within unit cell can be neglected since the porous foam sample is sufficiently thick. This means that each unit cell has a unique value of temperature in the same layer [26].

Other simplifications are described in the due course in the rest of the paper.

157 *2.3. Mathematical formulations*

158 *2.3.1 Basic formulations*

159 Based on the assumptions, the temperature difference between the two cells in

160 adjacent planes in *Y* direction is represented by equation:

161 $$\Delta T = \frac{T_h - T_c}{N_c} \quad (4)$$

162 where ΔT is the temperature difference between the two cells in adjacent planes, N_c

163 denotes the total number of cells in *Y* direction which is given by:

164 $$N_c = \frac{H}{d} \quad (5)$$

165 where *H* is the thickness of the porous medium sample. The temperature of the *i*th

166 (i=1,2,3… N_c) cell is:

167 $$T[i] = T_h - (i-1)\Delta T \quad (6)$$

168 Thus, the radiative conductivity k_r can be obtained by:

169 $$k_r = \frac{q_{r,net}}{(T_h - T_c)/H} \quad (7)$$

170 where $q_{r,net}$ is the net radiation heat flux.

171 The net radiation heat flux $q_{r,net}$ will be calculated based on the top void face *t* of

172 the *i*th cell. Since the radiation heat fluxes in both directions are not identical, the net

173 radiation heat flux can be mathematically expressed by the following equation:

174 $$q_{r,net} = q_r - q_r^- \quad (8)$$

175 where q_r is the radiation heat flux in the positive *Y* direction and q_r^- is the

176 radiation heat flux in the negative *Y* direction, respectively.

2.3.2 Formula derivation

Firstly, radiation in the positive *Y* direction is analysed, as radiation in the negative *Y* direction is familiar with that in positive *Y* direction. The total irradiation on the void face *t* of the *i*th cell (Fig. 2(b)) consists of both the emission and reflectance from the solid particles *1-4* to the void faces *s*, *b*. The total irradiation Q_r on *t* is given by:

$$Q_r = (Q_r)_{emission} + (Q_r)_{reflec\ tance} \tag{9}$$

where,

$$(Q_r)_{emission} = \sum_{j=1}^{4} l_j F_{jt} \cdot \varepsilon \sigma T^4 + l_b F_{bt} J_b + 2 l_s F_{st} J_s \tag{10}$$

In Eq. (11):

l_j (*j=1,2,3,4*) is the length of the *j*th solid particle within a unit cell, ε is the solid emissivity, σ is Stefan-Boltzmann constant equal to 5.669×10^{-8} W/m^{2}K^4, *T* is the temperature of the unit cell, l_b and J_b are the length and irradiation of the void face *b*, l_s and J_s are the length and irradiation of the void faces, *F* is the configuration factor.

The three terms on the right side of Eq. (11) are the emission on the void face *t* from four solid particles in four corners, bottom void face *b* and side void faces *s*, respectively.

$$(Q_r)_{reflec\ tance} = \sum_{j=1}^{4} \sum_{k=1,\, j \neq k}^{4} \rho l_j F_{jk} F_{kt} \cdot \varepsilon \sigma T^4 + \sum_{j=1}^{4} \rho l_b F_{bj} F_{jt} J_b + 2 \sum_{j=1}^{4} \rho l_s F_{sj} F_{jt} J_s \tag{11}$$

where $\rho = 1 - \varepsilon$ is the solid reflectivity. Similarly, the three terms on the right side of Eq. (12) represent the reflectance of the incident radiation on the solid particles from each other, bottom void face and two side faces, respectively.

It is noted that the specific surface area in the present 2D model is different compared with that in 3D structure, this may result in the emission deviation from solid particles in the calculation of radiation. In order to reduce this deviation, a new correction factor *C* is introduced to correct the emission from solid particles, which is defined as:

$$C = \frac{A_{sf,3D}}{A_{sf,2D}} \tag{12}$$

where $A_{sf,2D}$, $A_{sf,3D}$ are the specific surface areas in the present simplified 2D model and 3D model respectively.

For the 3D structure of the metal foam, according to [28], the specific surface area was defined as:

$$A_{sf,3D} = \frac{3\pi d_f [1 - e^{-(1-\phi)/0.04}]}{(0.59 d_p)^2} \tag{13}$$

where d_f is diameter of the strut.

For the present model, the specific surface area can be defined as the ratio of the total side length of solid particles to the area:

$$A_{sf,2D} = \frac{8a}{d^2} \tag{14}$$

Thus, the correction factor *C* can be derived as:

$$C = \frac{A_{sf,3D}}{A_{sf,2D}} = \frac{3\pi d_f [1 - e^{-(1-\phi)/0.04}] d^2}{8a(0.59 d_p)^2} = 1.0773\ \pi^{2.5}(1-\phi)^{-0.5}[1 - e^{-(1-\phi)/0.04}]\frac{d_f}{d_p} \tag{15}$$

Thus, the previous analysis needs to be reconsidered. The proposed correction factor *C* is added into the emission radiation term in Eqs. (11-12), then Eqs. (11-12) can be rewritten as:

$$(Q_r)_{emission} = \sum_{j=1}^{4} Cl_j F_{jt} \cdot \varepsilon\sigma T^4 + l_b F_{bt} J_b + 2 l_s F_{st} J_s \quad (16)$$

$$(Q_r)_{reflectance} = \sum_{j=1}^{4} \sum_{k=1, j\neq k}^{4} C\rho l_j F_{jk} F_{kt} \cdot \varepsilon\sigma T^4 + \sum_{j=1}^{4} \rho l_b F_{bj} F_{jt} J_b + 2\sum_{j=1}^{4} \rho l_s F_{sj} F_{jt} J_s \quad (17)$$

Considering the model is two-dimensional, the unit of Q is W/m.

For the purpose of convenience, the configuration factors can be analysed geometrically. The following formulations are used:

$$F_{12} = F_{21} = F_{13} = F_{31} = F_{34} = F_{43} = F_{24} = F_{42} = F_1 \quad (18)$$

$$F_{14} = F_{41} = F_{23} = F_{32} = F_2 \quad (19)$$

$$F_{1t} = F_{2t} = F_3 \quad (20)$$

$$F_{3t} = F_{4t} = F_4 \quad (21)$$

$$l_1 = l_2 = l_3 = l_4 \quad (22)$$

$$l_t = l_b = l_s \quad (23)$$

$$F_{s1} = F_{s3} = F_{b3} = F_{b4} = \frac{l_1}{l_s} F_3 \quad (24)$$

$$F_{s2} = F_{s4} = F_{b1} = F_{b2} = \frac{l_1}{l_s} F_4 \quad (25)$$

where l_t is the length of the top void face in the unit cell.

Radiation in the positive Y direction is given by:

$$q_r = \frac{Q_r}{l_t} \quad (26)$$

Substitute Eqs. (19-26) into Eq. (27), the radiation in the positive Y direction can be expressed in the following manner:

$$q_r = \frac{Q_r}{l_t} = C\frac{l_1}{l_t}(2 + 4\rho F_1 + 2\rho F_2)(F_3 + F_4)\varepsilon\sigma T^4$$

$$+ (F_{bt} + 4\frac{l_1}{l_t}\rho F_3 F_4)J_b + \left[2F_{st} + 2\frac{l_1}{l_t}\rho(F_3 + F_4)^2\right]J_s \quad (27)$$

For reducing Eq. (28), dimensionless coefficientsβ_1, β_2, β_3 are introduced and defined as:

$$\beta_1 = Cl_1(2 + 4\rho F_1 + 2\rho F_2)(F_3 + F_4)/l_t \quad (28)$$

$$\beta_2 = F_{bt} + 4l_1\rho F_3 F/l_t \quad (29)$$

$$\beta_3 = 2F_{st} + 2l_1\rho(F_3 + F_4)^2/l_t \quad (30)$$

Thus, Eq. (28) can be further reduced to:

$$q_r = \beta_1\varepsilon\sigma T^4 + \beta_2 J_b + \beta_3 J_s \quad (31)$$

In order to calculate the radiation in the positive Y direction q_r, J_b and J_s which are in the right side of Eq. (32) should be calculated firstly. Similarly, the irradiation from the void face s, J_s can be analyzed

$$J_s = C\frac{l_1}{l_s}(2 + 4\rho F_1 + 2\rho F_2)(F_3 + F_4)\varepsilon\sigma T^4$$

$$+ (F_{bt} + 4\frac{l_1}{l_s}\rho F_3 F_4)J_s + \left[F_{st} + \frac{l_1}{l_s}\rho(F_3 + F_4)^2\right]J_b \quad (32)$$

The quantity of J_s can be calculated from Eq. (33) which is written as following:

$$J_s = C\frac{l_1(2 + 4\rho F_1 + 2\rho F_2)(F_3 + F_4)/l_s}{1 - F_{bt} - 4l_1\rho F_3 F/l_s}\varepsilon\sigma T^4 + \frac{2F_{st} + 2l_1\rho(F_3 + F_4)^2/l_s}{1 - F_{bt} - 4l_1\rho F_3 F/l_s}J_b \quad (33)$$

Eq. (34) can be further written as:

$$J_s = \alpha_1\varepsilon\sigma T^4 + \alpha_2 J_b \quad (34)$$

where α_1 andα_2 are the dimensionless coefficients, defined as:

$$\alpha_1 = C\frac{l_1(2+4\rho F_1+2\rho F_2)(F_3+F_4)/l_s}{1-F_{bt}-4l_1\rho F_3 F/l_s} \tag{35}$$

$$\alpha_2 = \frac{2F_{st}+2l_1\rho(F_3+F_4)^2/l_s}{1-F_{bt}-4l_1\rho F_3 F/l_s} \tag{36}$$

Substitute Eq. (35) into Eq. (32), Eq. (32) can be further written as:

$$q_r = (\beta_1+\beta_3\alpha_1)\varepsilon\sigma T^4 + (\beta_2+\beta_3\alpha_2)J_b \tag{37}$$

2.3.3 Iteration process

For the convenience of iteration process, q_r, T, J_b of the ith unit cell can be rewritten as $q_r[i]$, $T[i]$, $J_b[i]$, thus, Eq.(38) can be rewritten as:

$$q_r[i] = (\beta_1+\beta_3\alpha_1)\varepsilon\sigma(T[i])^4 + (\beta_2+\beta_3\alpha_2)J_b[i] \tag{38}$$

As the bottom face b of the ith unit cell is the top face of the (i-1)th unit cell.

Therefore, the Eq. (39) can be expressed as:

$$q_r[i] = (\beta_1+\beta_3\alpha_1)\varepsilon\sigma(T[i])^4 + (\beta_2+\beta_3\alpha_2)q_r[i-1] \tag{39}$$

Similarly,

$$q_r[i-1] = (\beta_1+\beta_3\alpha_1)\varepsilon\sigma(T[i-1])^4 + (\beta_2+\beta_3\alpha_2)q_r[i-2] \tag{40}$$

$$q_r[i-2] = (\beta_1+\beta_3\alpha_1)\varepsilon\sigma(T[i-2])^4 + (\beta_2+\beta_3\alpha_2)q_r[i-3] \tag{41}$$

…

where the bottom face of the first unit cell is the bottom boundary of the porous medium sample with the temperature T_h, thus:

$$q_r[1] = (\beta_1+\beta_3\alpha_1)\varepsilon\sigma(T[i-2])^4 + (\beta_2+\beta_3\alpha_2)\varepsilon\sigma T_h^4 \tag{42}$$

Thus, the quantity of $q_r[i]$ can be calculated implementing an iterative procedure from the boundary.

In the case of the radiation flux in the negative y direction, it can similarly be written as:

$$q_r^-[i] = (\beta_1 + \beta_3\alpha_1)\varepsilon\sigma(T[i+1])^4 + (\beta_2 + \beta_3\alpha_2)J_b^-[i] \quad (43)$$

where $J_b^-[i]$ is the irradiation on void face *t* of *i*th unit cell from the top void face of the (*i+1*)th unit cell, as shown in Fig.2(b).

Similarly,

$$q_r^-[i] = (\beta_1 + \beta_3\alpha_1)\varepsilon\sigma(T[i+1])^4 + (\beta_2 + \beta_3\alpha_2)q_r^-[i+1] \quad (44)$$

$$q_r^-[i+1] = (\beta_1 + \beta_3\alpha_1)\varepsilon\sigma(T[i+2])^4 + (\beta_2 + \beta_3\alpha_2)q_r^-[i+2] \quad (45)$$

…

$$q_r^-[N_c] = \varepsilon\sigma T_c^4 \quad (46)$$

The determination of $q_r^-[i]$ is the same as that of $q_r[i]$. Then $q_{r,net}$ can be calculated by Eq. (9). Consequently, the equivalent radiative conductivity is determined by Eq. (8).

3. Determination of coefficients

In the analytical solution of the equivalent radiative conductivity, the dimensionless coefficients, i.e., β_1, β_2, β_3 and α_1, α_2 need to be determined. As previously mentioned, the coefficients are the functions of the configuration factors, geometric parameters and the solid reflectance according to Eqs. (29-31) and Eqs. (36,37). In order to determine these coefficients, the configuration factors, F_1, F_2, F_3, F_4, F_{bt} and F_{st}, should be firstly determined. The crossed strings method is utilized to calculate the

294 configuration factors for a two-dimensional geometric structure with known
295 geometric parameters of the unit cell.

296 As for the solid reflectance, it is recognized that the solid reflectance is related to
297 the emissivity ($\rho+\varepsilon=1$ for opaque material). However, the emissivity of a solid
298 material depends on many other factors such as temperature and orientation. The
299 influence of the emissivity on the radiation heat transfer is discussed in next section.

300 **4. Results and discussion**

301 *4.1. Model validation*

302 In the current work, the validation of the model is based on the FeCrAlY (Fe 75%,
303 Cr 20%, Al 5%, Y 2%) metallic foam produced via the sintering route which is
304 studied by Zhao et al. [23] and the test conditions employed for the current simulation
305 are listed in Table 1. Due to the fact that the real values of the geometric parameters
306 of the metal foam usually are different from that supplied by manufacturers, the
307 measured values instead of the nominal values will be considered. The currently
308 developed model will be evaluated through the comparison of the equivalent radiative
309 conductivity between the experimental data [23] and numerical results under the same
310 test conditions that shown in Table 1 based on the previous analytical models [25,26].

311 Figs. 3-6 show the comparison of the radiative conductivity versus temperature at
312 different pores per inch (PPI) and porosity between the present predicted results of
313 corrected model and experimental data [23] as well as numerical results using
314 previous models in [25,26]. The results in Figs. 3-6 clearly show that the proposed

model and model from reference [26] perform well in predicting the experimental data in all cases, while the initial model proposed by Zhao et al. [25] performs not well for S2, S4. The differences between the predicted results and experimental data as well as the current prediction results are reported in Table 2. And it is noted that there may have been a slight over-estimation or under-estimation of the radiative conductivity. This could be mainly due to the fact that the current model assumes uniform distribution of the solid particles in the porous media and uses the average particle diameter whereas in the real case the particle size is within a certain range. Despite this, it can be seen that in general there is a good agreement between the currently predicted and the experimental data.

Then the effects of the control parameters such as, correction factor, the number of the orders, the solid emissivity, temperature gradient, and the geometry on the radiative conductivity will be examined in detail.

4.2. Effect of correction factor

Fig. 7 shows the predicted radiative conductivity with and without the correction factor for the case of S1. It can be seen clearly that there is a large deviation between experimental data and predicted results for the case without correction factor. Thus, the contribution of the correction is significant. It reveals that the geometrical characteristics needs to be consistent with that in three-dimensional structure of metal foam to ensure the validity of the simplified model.

4.3. Effect of number of orders

As analysed in Section 2, the radiative conductivity is determined by implementing an iterative procedure which takes into account the irradiation from other unit cells up to the ones in contact with the boundaries. We define that the model has first-order accuracy if the *(i-1), i, (i+1), (i+2)*th unit cells are reserved which implies that the *i*th cell and *(i+1)*th cell share the face *t* that only accounts for the contributions from the adjacent neighbouring cells(*(i-1)*th, *(i+2)*th) in both directions. Geometrically, the face *t* is the central face within these four cells along y direction. Thus, the bottom face of the *(i-1)*th cell and the top face of *(i+2)*th cell are boundaries. Similarly, for second-order accuracy, one more unit cell in both directions is included in the calculation. For the other numbers of the orders, they can be defined in a same principle. Fig. 8 shows that the radiative conductivity of the sample 1 varies with the number of the order at two different temperatures, i.e. 550 K and 750 K at a solid emissivity of 0.6. It reveals that the numbers of the cells above and below the central face need to be considered to obtain the stable values of the radiative conductivity. Thus, in order to stabilize the calculated values of the radiative conductivity, the number of orders of 25 is used for the current model.

4.4. Effect of the solid emissivity

As previously mentioned, the effect of the solid emissivity on the radiative conductivity needs to be addressed. Generally, the emissivity of the steel varies between 0.3 and 0.8 [29]. Fig. 9 shows the effect of the solid emissivity on the values of the radiative conductivity at two temperatures of 550 K and 750 K. It is seen that

the value of the radiative conductivity increases with increasing solid emissivity even though a large emissivity can lead to a smaller reflectance. It reveals that the proportion of the emission in total radiation is relatively large. In addition, the effect of the solid emissivity on the radiative conductivity is significant at temperature of 750 K, while that is relatively mild at temperature of 550 K. The reason is that the emitting radiation is in proportion to the biquadrate of temperature. However, for the purpose of comparison, a solid emissivity of 0.6 is assumed in present work, which is consistent with the previous study of [25] and [26].

4.5. Effect of temperature gradient

For a fixed thickness with the same mean temperature, the effect of the temperature difference on the predicted radiative conductivity at fixed temperature of 750 K is shown in Fig.10. A specific mean temperature can be determined in different temperature difference between the top and bottom boundaries of the foam samples. It can also be concluded from Fig. 10 that the radiative conductivity is not sensitive to the temperature difference. In the current model, therefore, a 10 K temperature difference is used for the iterative procedure.

4.6. Effect of geometry

As mentioned in Section 2.1, the shape of the solid particles can be other simple geometries. In the current study, two shapes, i.e. circle, rhombus are assumed based on the same porosity and characteristic size in order to investigate the effect of the shape of solid particles, as shown in Fig. 11. The calculated results are shown in Fig.

12 for the case of S1. It can be seen that the shape of the solid particles has small effect on the thermal radiation in the present model. It is noted that different shapes of the solid particles may lead to different geometry structure, which implies that the configuration factors may be different. However, due to the large porosity of the metal foam, the influence of the different structures is insignificant.

Fig. 13 demonstrates the variation of the radiative conductivity with the change of the PPI for the same porosity of 95%. For comparison purposes, two PPI are used i.e. 30 and 60. Comparison shows that the radiative conductivity increases monotonously with decreasing PPI at the same temperature, such a result is due to the smaller PPI results in a bigger pore size. And the bigger pore size would lead to a large "penetration thickness" which implies that more heat can be directly transferred by thermal radiation to a deeper thickness of the foam before it decays to a lower level [25].

5. Conclusions

A newly developed two-dimensional model is employed for the calculation of the radiation heat transfer in highly porous open-cell metal foams and comparing these results with available experimental data as well as three-dimensional numerical solution proposed in the previous work. A new correction factor, C, is introduced for correcting the deviation of specific area between simplified two-dimensional structure and three-dimensional structure. The results demonstrated that using a two-dimensional analytical model instead of a three-dimensional approach leads to a

399 relatively minor discrepancy. Besides, the calculation is simpler than the
400 three-dimensional model because of the simpler determination of configuration
401 factors and coefficients due to the nature of the two-dimensional structure, which is
402 significant for engineering applications. The effect of the solid emissivity on the
403 radiative conductivity is more significant at higher temperature. The radiative
404 conductivity is not sensitive to the temperature difference during the iterative
405 procedure. The effect of the shape of the solid particle is observed and it is relatively
406 small. It is found that the samples with smaller PPI could lead to a higher value of
407 radiative conductivity. The correction factor C is found to be significant for the
408 present model. Overall, the main contribution of the proposed two-dimensional model
409 is the simplicity and convenience of calculation with good accuracy compared with
410 the previous three-dimensional model. In addition, the present model is also suitable
411 for vacuum condition. Future works are still needed to investigate the thermal
412 radiation in metal foam in atmospheric pressure. Besides, more experimental data of
413 different metal foams (material, PPI, porosity etc.) are needed to validate the present
414 model.
415
416 **Acknowledgements**
417
418 The authors would like to acknowledge the financial support from National Natural
419 Science Foundation of China (No. 51206164).

420 **References**

[1] C. Y. Zhao, Review on thermal transport in high porosity cellular metal foams with open cells, Int. J. Heat Mass Transfer, 55(13-14) (2012) 3618-3632.

[2] S. Y. Kim, J. W. Paek and B. H. Kang, Flow and heat transfer correlations for porous fin in a plate-fin heat exchanger, J Heat Trans- ASME, 122(3) (2000) 572-578.

[3] C. Albanakis, D. Missirlis, N. Michailidis, K. Yakinthos, A. Goulas, H. Omar, D. Tsipas and B. Granier, Experimental analysis of the pressure drop and heat transfer through metal foams used as volumetric receivers under concentrated solar radiation, Exp. Therm Fluid Sci., 33(2) (2009) 246-252.

[4] X. H. Yu, Z. Z. Wen, Y. Lin, S. T. Tu, Z. D. Wang and J. Y. Yan, Intensification of biodiesel synthesis using metal foam reactors, Fuel, 89(11) (2010) 3450-3456.

[5] A. Bhattacharya, V. V. Calmidi and R. L. Mahajan, Thermophysical properties of high porosity metal foams, Int. J. Heat Mass Transfer, 45(5) (2002) 1017-1031.

[6] K. Boomsma and D. Poulikakos, On the effective thermal conductivity of a three-dimensionally structured fluid-saturated metal foam, Int. J. Heat Mass Transfer, 44(4) (2001) 827-836.

[7] V. V. Calmidi and R. L. Mahajan, The effective thermal conductivity of high porosity fibrous metal foams, J Heat Trans-T Asme, 121(2) (1999) 466-471.

[8] Z. Dai, K. Nawaz, Y. G. Park, J. Bock and A. M. Jacobi, Correcting and extending the Boomsma-Poulikakos effective thermal conductivity model for

441 three-dimensional, fluid-saturated metal foams, Int. Commun. Heat Mass
442 Transfer, 37(6) (2010) 575-580.
443 [9] M. A. A. Mendes, S. Ray and D. Trimis, A simple and efficient method for the
444 evaluation of effective thermal conductivity of open-cell foam-like structures, Int.
445 J. Heat Mass Transfer, 66 (2013) 412-422.
446 [10] M. A. A. Mendes, S. Ray and D. Trimis, An improved model for the effective
447 thermal conductivity of open-cell porous foams, Int. J. Heat Mass Transfer, 75
448 (2014) 224-230.
449 [11] J. W. Paek, B. H. Kang, S. Y. Kim and J. M. Hyun, Effective thermal
450 conductivity and permeability of aluminum foam materials, Int. J.
451 Thermophysics, 21(2) (2000) 453-464.
452 [12] R. Singh and H. S. Kasana, Computational aspects of effective thermal
453 conductivity of highly porous metal foams, Appl. Therm. Eng., 24(13) (2004)
454 1841-1849.
455 [13] B. Dietrich, G. Schell, E. C. Bucharsky, R. Oberacker, M. J. Hoffmann, W.
456 Schabel, M. Kind and H. Martin, Determination of the thermal properties of
457 ceramic sponges, Int. J. Heat Mass Transfer, 53(1-3) (2010) 198-205.
458 [14] R. Coquard and D. Baillis, Numerical investigation of conductive heat transfer in
459 high-porosity foams, AcMat, 57(18) (2009) 5466-5479.

460 [15] P. Kumar and F. Topin, Simultaneous determination of intrinsic solid phase
461 conductivity and effective thermal conductivity of Kelvin like foams, Appl.
462 Therm. Eng., 71(1) (2014) 536-547.
463 [16] M. A. A. Mendes, V. Skibina, P. Talukdar, R. Wulf, U. Gross, D. Trimis and S.
464 Ray, Experimental validation of simplified conduction–radiation models for
465 evaluation of Effective Thermal Conductivity of open-cell metal foams at high
466 temperatures, Int. J. Heat Mass Transfer, 78 (2014) 112-120.
467 [17] E. Solorzano, M. Hirschmann, M. A. Rodriguez-Perez, C. Korner and J. A. de
468 Saja, Thermal conductivity of AZ91 magnesium integral foams measured by the
469 Transient Plane Source method, MatL, 62(24) (2008) 3960-3962.
470 [18] R. Wulf, M. A. A. Mendes, V. Skibina, A. Al-Zoubi, D. Trimis, S. Ray and U.
471 Gross, Experimental and numerical determination of effective thermal
472 conductivity of open cell FeCrAl-alloy metal foams, Int. J. Thermal Sciences, 86
473 (2014) 95-103.
474 [19] R. Coquard, D. Rochais and D. Baillis, Conductive and Radiative Heat Transfer
475 in Ceramic and Metal Foams at Fire Temperatures, Fire Technol., 48(3) (2010)
476 699-732.
477 [20] R. Coquard, D. Rochais and D. Baillis, Experimental investigations of the
478 coupled conductive and radiative heat transfer in metallic/ceramic foams, Int. J.
479 Heat Mass Transfer, 52(21-22) (2009) 4907-4918.

480 [21] R. Coquard, D. Baillis and J. Randrianalisoa, Homogeneous phase and
481 multi-phase approaches for modeling radiative transfer in foams, Int. J. Thermal
482 Sciences, 50(9) (2011) 1648-1663.
483 [22] M. Tancrez and J. Taine, Direct identification of absorption and scattering
484 coefficients and phase function of a porous medium by a Monte Carlo technique,
485 Int. J. Heat Mass Transfer, 47(2) (2004) 373-383.
486 [23] C. Y. Zhao, T. J. Lu, H. P. Hodson and J. D. Jackson, The temperature
487 dependence of effective thermal conductivity of open-celled steel alloy foams,
488 Mat Sci Eng a-Struct, 367(1-2) (2004) 123-131.
489 [24] C. Y. Zhao, T. J. Lu and H. P. Hodson, Thermal radiation in ultralight metal
490 foams with open cells, Int. J. Heat Mass Transfer, 47(14-16) (2004) 2927-2939.
491 [25] C. Y. Zhao, S. A. Tassou and T. J. Lu, Analytical considerations of thermal
492 radiation in cellular metal foams with open cells, Int. J. Heat Mass Transfer,
493 51(3-4) (2008) 929-940.
494 [26] G. Contento, M. Oliviero, N. Bianco and V. Naso, Prediction of radiative heat
495 transfer in metallic foams, Int. J. Thermal Sciences, 76 (2014) 147-154.
496 [27] G. Contento, M. Oliviero, N. Bianco and V. Naso, The prediction of radiation
497 heat transfer in open cell metal foams by a model based on the Lord Kelvin
498 representation, Int. J. Heat Mass Transfer, 76 (2014) 499-508.
499 [28] V.V. Calmidi, R.L. Mahajan, Forced convection in high porositymetal foams,
500 ASME J. Heat Transfer 122 (2000) 557 – 565.

[29] M. L. Hunt and C. L. Tien, Effects of Thermal Dispersion on Forced-Convection in Fibrous Media, Int. J. Heat Mass Transfer, 31(2) (1988) 301-309.

Fig. 1. Typical open-cell metallic foam morphology [25].

Fig. 2. (a) Two-dimensional idealized structure of porous medium; (b) Model foam structure and notations.

Fig. 3. Comparison between predicted results of present corrected model and experimental data, results of previous 3D models for S1.

Fig. 4. Comparison between predicted results of present corrected model and experimental data, results of previous 3D models for S2.

Fig. 5. Comparison between predicted results of present corrected model and experimental data, results of previous 3D models for S3.

Fig. 6. Comparison between predicted results of present corrected model and experimental data, results of previous 3D models for S4.

Fig. 7. Effect of correction factor on radiative conductivity for S1.

Fig. 8. Radiative conductivity vs. the number of orders at fixed solid emissivity of 0.6 and different temperatures for S1.

Fig. 9. Radiative conductivity vs. solid emissivity at different temperatures for S1.

Fig. 10. Radiative conductivity vs. temperature difference at fixed mean temperature for S1.

Fig. 11. Different shapes of solid particle.

Fig. 12. Effect of shape of solid particle on radiative conductivity for S1.

Fig. 13. Radiative conductivity vs. temperature at different PPI.

Table 1

Geometric properties of different foam samples [26].

	Sample			
	S1	S2	S3	S4
Pores per inch (PPI)	30	30	60	60
Nominal porosity (%)	95	90	95	90
Measured porosity (%)	95.9	90.7	94.5	90.8
Nominal cell size(mm)	0.847	0.847	0.423	0.423
Measured cell size(mm)	1.999	2.089	0.975	0.959
Equivalent cell size(mm)	1.772	1.851	0.864	0.850
Measured diameter of the strut(mm)	0.215	0.267	0.124	0.154

Table 2

Differences between predicted results and experimental data.

Sample	Zhao's model [25]	Contento's model [26]	Present corrected model
S1	-48.16%	-17.35%	-12.49%
S2	485.95%	63.37%	35.57%
S3	-19.14%	23.98%	-19.23%
S4	205.50%	-13.17%	-7.07%